arXiv:2410.21629v2 [cs.CV] 28 Feb 2025

OFER: Occluded Face Expression Reconstruction

Pratheba Selvaraju
University of Massachusetts, Amherst

Victoria Fernandez Abrevaya
Max Planck Institute for Intelligent Systems

Timo Bolkart
Google Research

Rick Akkerman
University of Amsterdam

Tianyu Ding, Faezeh Amjadi, Ilya Zharkov
Microsoft Research

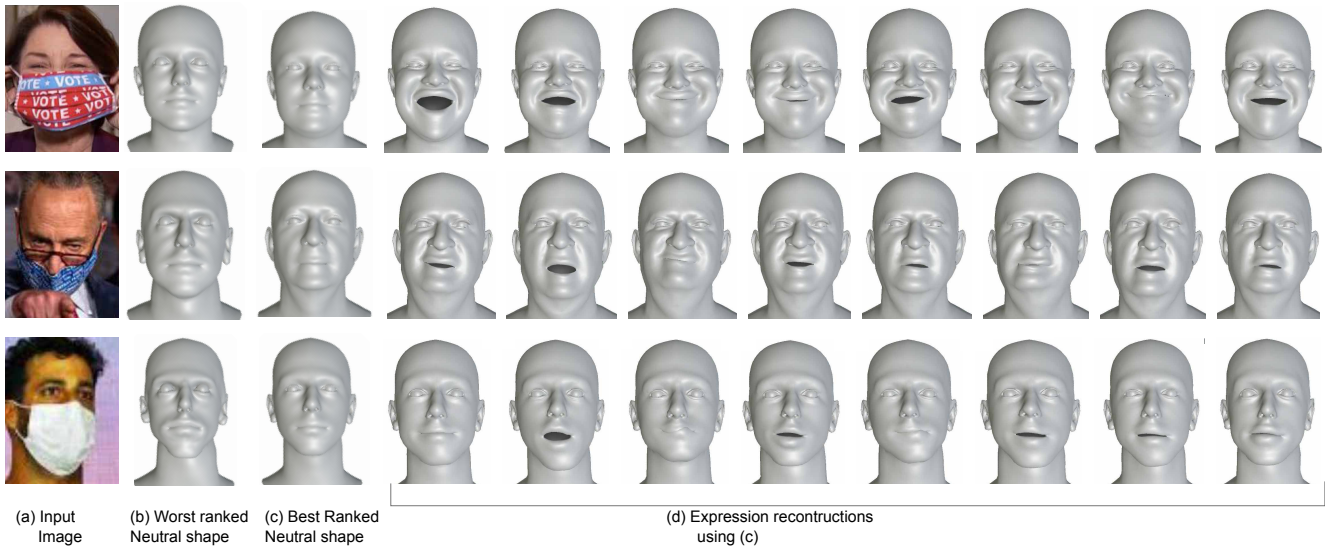


Figure 1. **Reconstructions generated by OFER.** Our method can reconstruct faces from a single image under hard occlusions (a), providing multiple solutions with diverse expressions that align with the input image (d). We use two diffusion models that denoise shape and expression parameters of FLAME conditioned on the image. A novel ranking mechanism selects an optimal identity (c) from the generated set of shapes, on top of which the expression variants are applied to obtain the final results.

Abstract

Reconstructing 3D face models from a single image is an inherently ill-posed problem, which becomes even more challenging in the presence of occlusions. In addition to fewer available observations, occlusions introduce an extra source of ambiguity where multiple reconstructions can be equally valid. Despite the ubiquity of the problem, very few methods address its multi-hypothesis nature. In this paper we introduce OFER, a novel approach for single-image 3D face reconstruction that can generate plausible, diverse, and expressive 3D faces, even under strong occlusions. Specifically, we train two diffusion models to generate the shape and expression coefficients of a face parametric model, conditioned on the input image. This approach captures the multi-modal nature of the problem, generating a distribution of solutions as output. However, to maintain consistency across diverse expressions, the challenge is to select the best matching shape. To achieve this, we propose a novel ranking mechanism that sorts the outputs of the shape diffusion network based on predicted shape accuracy scores. We evaluate our method using standard benchmarks and introduce CO-545, a new protocol and dataset designed to assess the accuracy of expressive faces under occlusion. Our results show improved performance over occlusion-based methods, while also enabling the generation of diverse expressions for a given image.

[1]Project website: https://ofer.is.tue.mpg.de/

1. Introduction

3D face reconstruction from a single image is crucial for creating life-like digital avatars and is used in numerous applications such as illumination-invariant recognition [60], medical imaging [37], and telepresence [30]. The task is an inherently challenging inverse problem, with difficulties posed by depth ambiguity, variations in lighting, diverse facial expressions, and pose [14].

The problem becomes even more challenging when images are subjected to *occlusions*, as shown in Fig. 1. The main difficulty arises from the face being only partially visible, introducing an additional source of ambiguity: the occluded areas can now correspond to an infinite number of valid shapes, making it a *multi-hypothesis reconstruction* problem. Occlusions are very common in images captured in uncontrolled environments due to factors such as hair, accessories, medical masks, or even strong profile poses and head rotations (*e.g*. Fig. 9). Despite its prevalence, reconstruction under such conditions has seldom been addressed.

3D face reconstruction typically involves recovering the parameters of a statistical 3D facial model, such as the 3D Morphable Model (3DMM) [4], either via model fitting [1, 4, 24] or regression [9, 12, 22, 51]. While these works may handle milder occlusions depending on their training data, their performance deteriorates significantly under more severe obstructions (see *e.g*. Fig. 2). A few methods have been specifically proposed to address the challenge of occluded faces [13, 17, 18, 31]. Most offer a unique solution due to their deterministic nature, ignoring the multi-hypothesis aspect of the problem [17, 18, 31]. An exception to this is Diverse3D [13], which employs Determinantal Point Process (DPP) [29] to sample a diverse set of outputs. While DDP is designed to capture the diversity of the data, it fails to adequately represent the underlying distribution of facial geometry, often resulting in unrealistic and exaggerated reconstructions as shown in Fig. 2.

To ensure plausible face reconstructions while addressing the challenges of diverse sampling, we introduce OFER, a novel method for reconstructing 3D faces under occlusions. At its core, OFER employs two denoising diffusion probabilistic models (DDPMs) [26] to generate the shape and expression coefficients of the FLAME [32] parametric face model, conditioned on the input image. The ability of diffusion models to learn the underlying data distribution enables OFER to produce multiple plausible hypotheses. We leverage two pre-trained face image recognition networks as image encoders, and following MICA [59], train our models using only a small dataset of paired 2D-3D data.

Generating diverse solutions is crucial for reconstructing faces under occlusions. Equally important is selecting a unique, consistent shape that best represents the face in the image across all generated expressions. This is achievable since identity is generally better defined under occlusions.

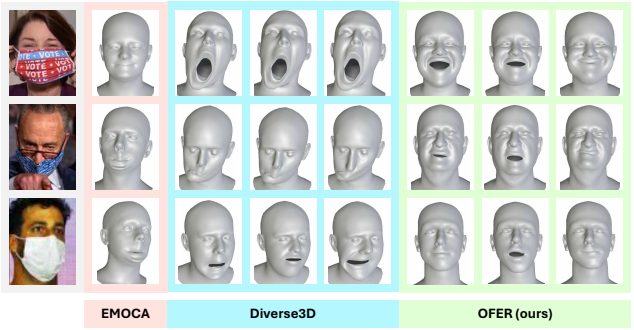


Figure 2. **Comparison against expression reconstruction methods.** We show results from EMOCA [9] (pink); samples generated by Diverse3D [13] (blue); and samples generated by our method (green). EMOCA can only reconstruct a single solution due to its deterministic nature, while Diverse3D shows non-plausible faces. OFER (our method) generates diverse 3D faces with plausible expressions.

To achieve this, we propose a novel **ranking mechanism** that evaluates and ranks the samples generated by the shape diffusion network, effectively filtering out poor quality samples. Specifically, given an input image along with N generated shape samples, the ranking network scores and ranks the candidates, selecting the top-ranked one. To the best of our knowledge, such a ranking mechanism as selection process for diffusion models has not been considered before.

To evaluate our approach, we introduce a new dataset and evaluation protocol, CO-545, derived from the CoMA dataset [42]. CO-545 includes 545 ground-truth pairs of occluded images and corresponding FLAME non-occluded 3D vertices. Experimental results show that our method effectively generates multiple hypotheses for single in-the-wild occluded images, achieving superior quality and diversity on CO-545. Additionally, when evaluated on the NoW benchmark [47], our method demonstrates improved performance with the ranking-selection mechanism.

In summary, our contributions are the following:

- A new method for occluded 3D face reconstruction using DDPMs, which outputs multiple 3D face shape and expression hypotheses, overcoming the limitations of deterministic methods.
- A novel ranking mechanism that scores and selects the optimal 3D face shape from reconstruction candidates generated by the shape network.
- A new validation dataset, CO-545, for the quantitative evaluation of occluded face reconstruction, addressing the lack of existing evaluation protocols.

2. Related Work

3D face reconstruction from a single image. 3D face reconstruction from a single image has been a key research area for several decades [19], with approaches broadly cat-

egorized into model-free [2, 11, 16, 21, 27, 45, 48, 55] and model-based methods [9, 22, 43, 56, 59]. Model-free approaches estimate 3D geometry directly from images, while model-based ones recover the low-dimensional parameters of a statistical model of the 3D face such as BFM [39] or FLAME [32]. To overcome the lack of large-scale datasets with paired images and 3D models, recent trends have shifted towards self-supervised learning [9, 12, 22, 43, 50], using landmark re-projection and/or photometric error. These works can yield suboptimal results when landmarks are missing or when color information is compromised due to occlusions. Alternatively, MICA [59] uses a small dataset of paired 2D-3D data to map an image embedding from a face recognition network [10] to the FLAME shape parameters. This technique achieves state-of-the-art results for neutral face shape reconstruction but does not support expressive faces.

3D face reconstruction from occluded images. A few works have specifically addressed the problem of reconstructing faces under occlusion. Egger et al. [17, 18] proposed a probabilistic optimization approach that simultaneously solves for model parameters and segmentation regions using an expectation–maximization approach. FOCUS [31] follows a similar idea within a self-supervised learning strategy. These methods prioritize obtaining valid reconstructions for the non-occluded regions but do not address the ambiguity of the problem, which requires a distribution of solutions. Recently, Diverse3D [13] tackled this by employing a mesh-based variational autoencoder (VAE) for shape completion, combined with Determinantal Point Process (DPP) [29] for sampling diverse solutions in expression space. However, the method often results in unrealistic and exaggerated reconstructions (see Fig. 2), since DDP is not designed to capture the statistical properties of the data.

Learning to Rank. Ranking plays an essential role in Information Retrieval [34], commonly used for sorting documents by relevance [25, 28], image search [38], and recommendation systems [35]. Learning to Rank methods [34] perform this task by making use of supervised machine learning. RankGAN [33] uses ranking as a rewarding mechanism to train a language generator to produce higher-quality descriptions. Some recent works such as T5 [58] focus on text ranking with large language models, and incorporate ranking losses as a fine-tuning tool to optimize model performance. To the best of our knowledge, ranking has not been explored in the context of diffusion models to select an optimal sample.

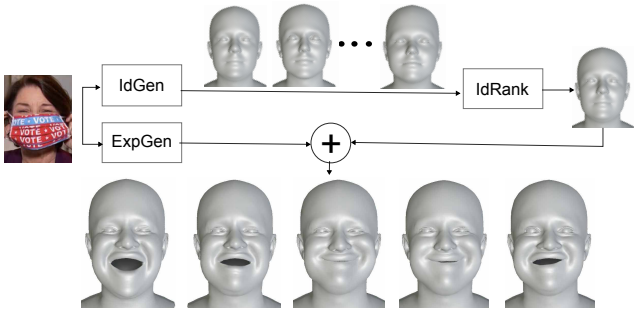


Figure 3. **Overview of OFER.** Given an input image, the *Identity Generative Network* (IdGen) samples N shape parameters. The reconstructed shapes are then passed to the *Identity Ranking Network* (IdRank) to select a unique identity. Finally, the *Expression Generative Network* (ExpGen) generates N expression parameters, which are combined with the selected shape to output *diverse and expressive face reconstructions* (bottom row).

3. Method

Our method takes as input a single-view image of an occluded face and generates a *set* of 3D faces as output. The goal is to produce reconstructions that explore a *diverse range of expressions* in the occluded areas, while accurately capturing the visible regions of the input image.

OFER is structured around three key components. First, the *Identity Generative Network* (IdGen, Fig. 4 and Sec. 3.2), a DDPM conditional diffusion model, outputs a set of FLAME [32] shape coefficients, recovering a distribution of plausible neutral 3D faces. Next, the *Identity Ranking Network* (IdRank, Fig. 5 and Sec. 3.3), a small MLP, evaluates and ranks the shape samples given by the previous network. This step selects a unique shape coefficient that best explains the image. Finally, the *Expression Generative Network* (ExpGen, Fig. 4 and Sec. 3.4), another conditional DDPM network, generates a diverse set of FLAME expression coefficients. We use default DDPM framework [26] with DDPM sampler with 1000 sampling time steps for both IdGen and ExpGen. The three networks are conditioned on the same input image. By combining the selected shape coefficient with the set of expression hypotheses, we obtain the final set of 3D reconstructions. The overall architecture of OFER is shown in Fig. 3. We detail each of its components in the following sections.

3.1. Preliminaries

FLAME Model. FLAME [32] is a parametric 3D face model combining separate shape and expression spaces to form a 3D head mesh M with $n = 5023$ vertices. Given the shape $S \in \mathbb{R}^{|S|}$, expression $E \in \mathbb{R}^{|E|}$, and pose $P \in \mathbb{R}^{|P|}$ parameters, FLAME produces a mesh M as

$$M(S, E, P) = \text{LBS}\big(\mathcal{T}(S, E, P), \mathcal{J}(S), P, \mathcal{W}\big), \quad (1)$$

where LBS is the linear blend skinning function using weights $\mathcal{W} \in \mathbb{R}^{4\times n}$ and joint regressor $\mathcal{J}(S) \in \mathbb{R}^{3K}$, and $T(S,E,P) = \mathcal{T} + \mathcal{B}_S(S) + \mathcal{B}_E(E) + \mathcal{B}_P(P)$ deforms a template mesh $\mathcal{T}$ using the shape $\mathcal{B}_S$, expression $\mathcal{B}_E$ and pose-corrective $\mathcal{B}_P$ blendshapes. FLAME uses $|S| = 300$ dimensions for shape and $|E| = 100$ dimensions for expression.

Denoising Diffusion Probabilistic Model (DDPM). The underlying mechanism of DDPM is the transformation of an unknown data distribution, $p(X) \in \mathcal{R}^d$ into a simple known distribution. Here, X represents the data from the underlying distribution. This transformation is achieved by iteratively applying a transition kernel q via a Markov chain process with infinitesimal time steps, ensuring a stationary distribution at each time step t i.e $x_t \sim q(x_t|x_{t-1}), \forall t > 0$ where $x \in X$. DDPM models these transformations by parameterizing a neural network to captures complex dependencies in the data by modeling the sequential evolution of the data distribution. In the work of Sohl et al.[49], the known distribution is set as gaussian with a decaying variance schedule $\beta_t \in \mathcal{R}$ such that $q(x_t|x_{t-1} = \mathcal{N}(x_t; \sqrt{1-\beta_t}x_{t-1}, \beta_t I); q(x_T) = \mathcal{N}(x_T; 0, I)$ due to its simplicity and tractability. Denoising in DDPM involves reversing this process by starting with unit gaussian noise and attempting to model the underlying data distribution $p'(X)$.

Learning-based Ranking. Ranking is an important technique used in the information retrieval domain to retrieve relevant documents given a query. There are three primary learning-based ranking techniques [34]: pointwise, pairwise and listwise. The pointwise model takes in a single query(q)-document(d_i) pair and gives the relevance score (s_i) of each in isolation, which requires the ground-truth score: $\bar{r}(q, d_i) = s_i$. Pairwise ranking methods compare two documents against each other based on importance and relevance to the query: $\bar{r}(q, d_i, d_j) = P(d_i \triangleright d_j)$. Finally, listwise ranking [41] generates an optimal order of a list of documents by calculating the importance score of each: $\bar{r}(q, d_i, \ldots, d_n) = (r_1, \ldots, r_n)$, which is the method we adopt in our network.

3.2. Identity Generative Network (IdGen)

The first step of OFER is to generate a set of FLAME shape coefficients, S. The identity network ϵ_θ^S (Fig. 4, top) consists of a 1-dimensional U-Net [44] with self-attention layers that is trained to transform unit Gaussian noise $s_T \sim \mathcal{N}(0, I_{300})$ into $s_0 = S$ through reverse time-steps $t = T..0$.

The input image is used as condition by encoding it into a 512-dimensional feature vector $c_a \in \mathbb{R}^{512}$ using the ArcFace [10] encoder. Following MICA [59], we freeze all layers of the ArcFace encoder except the last, such that the encoded features can be fine-tuned during training. During sampling, we generate a set of N noise vectors $\{s_T^i \in \mathbb{R}^{300}\}_{i=1}^N$ and iteratively denoise them using ϵ_θ^S to obtain the FLAME shape coefficients, $\{s_0^i = \hat{S}_i \in \mathbb{R}^{300}\}_{i=1}^N$. We optimize the parameters θ by minimizing the following loss function L_ε:

$$L_\varepsilon(\theta) = \mathbb{E}_t\Big[\mathbb{E}_{s_0,\varepsilon}[|\epsilon_\theta^S(s_t) - \varepsilon_t|]\Big]. \quad (2)$$

where ε_t is fixed Gaussian noise with variance proportional to the linear time step t [26]. Due to the nature of diffusion models, each generated sample $\hat{S}_i$ exhibits plausible variations in the occluded regions, capturing the variance in the input data.

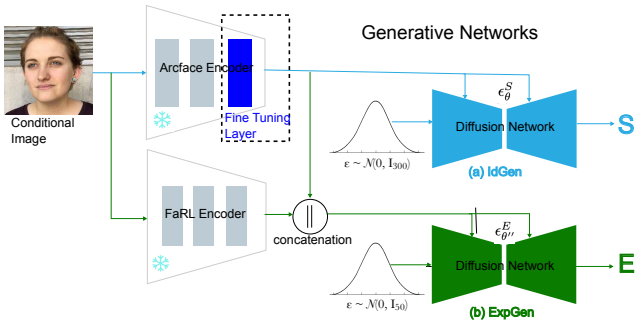


Figure 4. **Overview of the identity and expression generative networks** (IdGen, in blue, and ExpGen, in green). For IdGen, the input image is encoded into a 512-dimensional embedding using ArcFace [10]. This serves as a condition for the 1D U-Net diffusion network, which is trained to denoise 300-dimensional noise into FLAME shape coefficients, S. For ExpGen, the input image is encoded into a 1024-dimensional embedding using the FaRL [57] and ArcFace [10] encoders. The embedding serves as a condition for the 1D U-Net diffusion network, which is trained to denoise 50-dimensional noise into FLAME expression coefficients, E.

3.3. Identity Ranking Network (IdRank)

Our goal is to generate a set of 3D faces with diverse expressions that align with the input occluded image. While expressions can vary, we would like here to preserve a unique and consistent identity across all samples. This approach is motivated by three main observations. First, we noticed that shape coefficients display much less variability than expression coefficients, as images typically contain more cues for the expression-independent facial features. Second, we noticed in our experiments that, when computing the reconstruction error for the N generated samples, the minimum value is on-par to state-of-the-art methods (see supplementary material). Since identity is typically more defined than expression, a method capable of selecting this optimal sample would be advantageous. Finally, even in cases of severe occlusions where identity features may be less discernible, having a method that effectively filters out poorly generated

samples is important for practical applications.

Towards this end, we introduce IdRank, a network specifically designed to rank the outputs of IdGen in order to select those that best preserve the facial structure of the input image.

Ranking framework. The overall architecture of IdRank is shown in Fig. 5. Given a pool of N candidate shapes generated by IdGen, the goal is to select the one closest in distance to the ground-truth neutral shape (available during training). To achieve this, we train a *ranking* network $R_{\theta'}$ that goes from a list of v face vertices (derived from the shape coefficients) to a scalar p representing the probability that the sample matches the ground truth. We then apply the network $R_{\theta'}$ over the N samples, ranking each based on their scores and selecting the highest-scored sample.

Before passing the mesh to the network, we remove the vertices corresponding to the back of the head since they are rarely visible in the image, and their inclusion in the error computation might lead to spurious results.

The number of candidates N is an important hyper-parameter, as it defines a trade-off between computational complexity and reconstruction error –a large value of N means that the actual ground-truth shape has more chances of being generated, but incurs in a significantly higher computational cost. We empirically choose here $N = 100$ (see supplementary material).

Generating ground-truth data. During training, we generate the ground-truth data for ranking in an online fashion as follows. Given an image I together with its ground-truth FLAME mesh $M_{GT} \in \mathbb{R}^{5023}$, we first sample N shape parameters $\{\beta_i\}_{i=1}^{N}$ using IdGen (with gradient back-propagation disabled). We then reconstruct the neutral face vertices using Eq. (1), yielding a set of mesh candidates $\mathcal{M} = \{M_i = M(\beta, \mathbf{0}, \mathbf{0}) \in \mathbb{R}^{5023}\}_{i=1}^{N}$. From the set $\mathcal{M}$ as well as the ground-truth mesh M_{GT} we retain only the frontal vertices using a pre-computed mask, resulting in $\mathcal{M}^{\text{frontal}} = \{\hat{M}_i \in \mathbb{R}^{n'}\}_{i=1}^{N}$ and $M_{GT}^{\text{frontal}} \in \mathbb{R}^{n'}$ ($n' < 5023$). Finally, we compute the error between each $\hat{M}_i$ and M_{GT}^{frontal} to produce the following set:

$$\mathcal{D}_{GT} = \{|\hat{M}_i - M_{GT}^{\text{frontal}}|\}_{i=1}^{N}. \tag{3}$$

with $|\cdot|$ the L1 norm.

We empirically observed that removing the mean $\mu_{\mathcal{M}} = \frac{1}{N}\sum_{i=1}^{N}\hat{M}_i$ from the set $\mathcal{M}^{\text{frontal}}$ reduces redundancy and helps convergence of the network. Hence, we transform $\mathcal{M}_{\text{frontal}}$ into a zero-centered set of residual meshes $\mathcal{M}_{\text{centered}}$ via:

$$\mathcal{M}_{\text{center}} = \{M_i' = (\hat{M}_i - \mu_{\mathcal{M}})\}_{i=1}^{N}. \tag{4}$$

The final training set for image I is defined as the list of pairs $\mathbf{X} = [(\mu_{\mathcal{M}}, M_i')]_{i=1}^{N}$, obtained by sorting the values in $\mathcal{D}_{GT}$ in ascending order.

Learning to rank facial shapes. The ranking network $R_{\theta'}$ is a small MLP that takes as input a single pair $(\mu_{\mathcal{M}}, M_i')$ and is trained to predict a sample score d_i. It is conditioned on a 1024-dimensional feature vector $c_R = (c_a \| c_f)$, formed by concatenating features from the ArcFace (c_a) [10] and FaRL (c_f) encoders [57], designed for facial analysis tasks. The network is run N times producing $\mathcal{D} = \{d_1, \ldots, d_N\}$ scores, which are then passed through a softmax operator to transform them into probabilities, $P = \text{softmax}(\mathcal{D}) = \{p_i = \frac{e^{d_i}}{\sum_{j=1}^{N} e^{d_j}}\}_{i=1}^{N}$. The ground-truth distance values $\mathcal{D}_{GT}$ are also passed through a softmax operator, $\mathcal{D}'_{GT} = \text{softmax}(\mathcal{D}_{GT})$. Finally we compute the cross-entropy loss between the two distributions P and $\mathcal{D}'_{GT}$:

$$L_{\mathcal{D}'_{GT},P}(\theta') = -\sum_{i=1}^{N} \mathcal{D}'_{GT}(i)\log(p_i). \tag{5}$$

Inference. During inference, we select the sample with the highest probability score as the optimal sample, denoted as S_R. While multiple samples may have equal probability scores, their ordering in such cases would be rather random. In that case, we choose the first-ranked sample from this list of equally high probability samples.

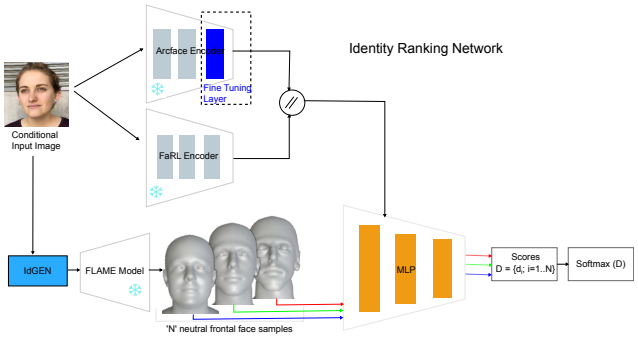


Figure 5. **Identity Ranking Network**. Given the N shape coefficients from IdGen, we reconstruct the neutral meshes using FLAME. Each mesh is passed through a 5-layer MLP to compute a score, conditioned on the input image using the ArcFace [10] and FaRL [57] encoders. The N scores are then converted into probabilities using softmax. The ranking order of the sorted scores is compared against the ranking of the sorted reconstructed errors, and the network is trained to match them.

3.4. Expression Generative Network (ExpGen)

The expression network $\epsilon_{\theta''}^{E}$ architecture (Fig. 4, bottom) closely follows that of IdGen, employing the conditional

DDPM framework to generate the first 50 components of the FLAME expression coefficients. It is conditioned on a 1024-dimensional feature vector, similar to IdRank.

During sampling, the network initializes from unit Gaussian noise $\varepsilon_T \in \mathbb{R}^{50}$ and iteratively denoises towards the FLAME expression parameters, $e_0 \in \mathbb{R}^{50}$. The parameters θ'' are optimized by minimizing the loss function Eq. (6)

$$L_\varepsilon(\theta'') = \mathbb{E}_t\Big[\mathbb{E}_{e_0,\varepsilon}[|\epsilon_\theta^E(e_t) - \varepsilon_t|]\Big]. \quad (6)$$

4. Experiments and Evaluations

In this section, we present qualitative and quantitative evaluation results for OFER. We begin by introducing the datasets used for training and testing, including the proposed CO-545 dataset, which we specifically designed to evaluate performance on occluded images (Sec. 4.1). Next, we provide evaluation metrics and experimental results on IdGen and IdRank (Sec. 4.2), followed by a similar analysis for the final reconstructions with ExpGen (Sec. 4.3).

4.1. Datasets

Training data. We train IdGen with the Stirling [23], FaceWarehouse [7], LYHM [8], and Florence [3] datasets, which contain 2D-3D ground-truth pairs of images and corresponding registered FLAME shape coefficients. The same four datasets are used to train IdRank. For ExpGen we use the FaMoS (Facial Motion across Subjects) [5] dataset, which offers paired image and FLAME 3D meshes of faces in motion. The shape and expression coefficients were provided by the FaMos authors.

The CO-545 dataset. To evaluate reconstruction of expressive faces under occlusions, we propose a new dataset built on top of the CoMA dataset [42]. The CO-545 validation dataset comprises 545 frontal face images (no profile or rotated head views) synthetically occluded (hand, face, and random) across 11 subjects taken from COMA [42]. For each image we identify the sets of occluded and unoccluded vertices, and evaluate them using separate metrics. More details can be found in the supplementary material.

Testing data. We evaluate the final expressive reconstructions using the dataset provided by Dey et al. [13] ("Dey Dataset"), as well as the CO-545 dataset. Additionally, we test on the real-world hard occlusion images dataset provided by Erakiotan et al. [20], which does not have any 3D ground truth data. We additionally evaluate the quality of neutral shape reconstructions using the occluded and unoccluded subsets of the NoW benchmark [47]. Note that we do not have access to the occluded/unoccluded split for the testing set, and hence provide results mainly for the validation set. Additional comparisons on the test set are included in the supplementary material.

4.2. Evaluation on IdGen and IdRank

We first evaluate the accuracy of the neutral mesh reconstructions provided by the IdGen network, as well as the ranked samples according to IdRank. We trained IdGen for 400 epochs with a batch size of 128 on an RTX 8000 GPU. The entire training process spans one GPU day. IdRank was trained for 120 epochs with a batch size of 32 on a Titan X GPU. The training process ran for 20 epochs per day, converging over the course of 6 days.

Baselines and Metrics. Since OFER is designed to provide multiple solutions, we establish a baseline by randomly sampling FLAME shape coefficients from its parametric space. We evaluate our approach on the NoW validation benchmark, which allows separate measurement for the occluded and unoccluded subsets of the dataset. We compare our method to standard reconstruction techniques as well as state-of-the-art occlusion-based approaches, Diverse3D [13] and FOCUS [31]. Our evaluation metrics include the mean, median, and standard deviation of the mean square error (MSE) relative to the ground-truth mesh.

Results. Fig. 6 and Fig. 7 present qualitative results of 3D shape reconstruction, alongside comparisons with the state-of-the-art neutral face reconstruction method MICA [59] and the occluded face reconstruction method by Dey et al. [13], Diverse3D. In Fig. 6 we observe that, despite mild occlusions, OFER can recover accurate shapes with distinctive features (e.g., cheeks in the first row and the head length in the second row). We show an example of extreme occlusion in Fig. 7, where we reconstruct two images of the same person wearing a face mask, alongside a minimally occluded reference image. We observe that OFER, and in particular the top-ranked sample, produces plausible results for the two masked images.

For quantitative evaluation, we use the NoW benchmark dataset [47], with the results presented in Tab. 2. Our method achieves a lower average error across all reconstructed samples compared to other state-of-the-art occlusion-based approaches. In addition, the shapes generated by IdGen can achieve competitive results with standard reconstruction methods, as shown by the minimum reconstruction error obtained over all samples (OFER-min).

Ablation. To highlight the effectiveness of ranking in improving the search space and in selecting high-quality samples, we conducted an ablation study, with results presented Tab. 1. In row (a), we show the results of generating 200 and 1000 random FLAME samples, while row (d) presents the results from OFER. The "ideal lowest error" column corresponds to an ideal ranking (i.e. the minimum error within the samples). Even with an increased number of random

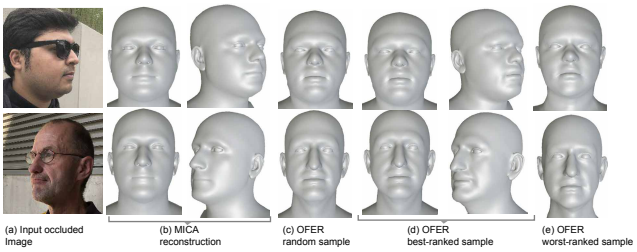


Figure 6. **Neutral face reconstruction on occluded images**. For (a) the given occluded input image, (b) shows the reconstructed shape provided by MICA [59]; (c) is one of the generated samples from our method; (d) and (e) are the best and worst-ranked samples, respectively, as selected by the ranking network.

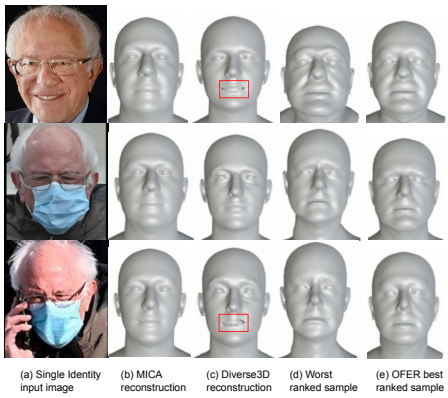


Figure 7. **Neutral face reconstruction on a single identity**. For (a) the given input image, (b) shows the reconstructed shape provided by MICA [59]; (c) shows the reconstructed shape provided by Diverse3D [13]; (d) and (e) are the worst and best-ranked samples as selected by the ranking method.

hypotheses (1000 samples), finding a good reconstruction in this space remains less likely, as indicated by the higher error in the ideal ranking scenario (0.81 with OFER vs 0.90 with FLAME), showcasing the improved search space when ranking is applied to IdGen. In row (b) we show the results of ranking a set consisting of 50% random FLAME samples and 50% OFER reconstructions; row (c) reflects the same for an $80/20$ split. This mimics a scenario where the samples to rank include both correct solutions and high-error ones. Here, the ranked results (1st and 2nd columns) are consistently lower than the average error (3rd column), highlighting its effectiveness in selecting low-error samples. This is further supported by qualitative evidence in Fig. 8.

We further demonstrate the network's ability to identify subtle differences to select top-ranked sample with lower error than the lower ranked samples, as shown in the color coded error map in Fig. 10 in the supplement.

Samples	Ideal lowest error Sample			Ranked Sample			Average of all Samples		
	Med ↓	Mean ↓	std ↓	Med ↓	Mean ↓	std ↓	Med ↓	Mean ↓	std ↓
(a)FLAME(200 - 1k)	(1.00 - 0.90)	(1.31 - 1.20)	(1.18 - 1.11)	NA	NA	NA	1.75	2.19	1.86
(b)FLAME(50)+OFER(50)	0.84	1.09	0.95	1.08	1.44	1.32	1.33	1.79	1.62
(c)FLAME(80)+OFER(20)	0.86	1.10	0.97	1.34	1.81	1.65	1.60	2.06	1.84
(d)OFER(100)	**0.81**	**1.05**	**0.92**	**0.98**	**1.21**	**1.01**	**1.02**	**1.25**	**1.04**

Table 1. **Ablation study on the importance of ranking.** *Ideal Lowest Error Sample* refers to the sample with the lowest median MSE. *Ranked Sample* is the optimal sample selected by the Ranking Network from all samples generated by the IdGen. *Average of All Samples* represents the average error across all generated samples. "NA" in the Ranked Sample column for the 200-1K range indicates that our network, which was trained on 100 samples, cannot validate these larger sample sizes.

Method	Unoccluded			Occluded			Both		
	Med	Mean	std	Med	Mean	std	Med	Mean	std
FLAME	1.79	2.24	1.89	1.80	2.26	1.91	1.79	2.25	1.90
Deep3D [12]	1.33	1.67	1.41	1.40	1.73	1.41	1.36	1.70	1.41
DECA [22]	1.18	1.47	1.24	1.29	1.56	1.29	1.17	1.46	1.25
MICA (4DS) [59]	n/a	n/a	n/a	n/a	n/a	n/a	1.02	1.25	1.05
MICA (8DS) [59]	n/a	n/a	n/a	n/a	n/a	n/a	0.90	1.11	0.92
TokenFace [56]	n/a	n/a	n/a	n/a	n/a	n/a	**0.79**	**0.99**	**0.85**
FOCUS [31]	1.03	1.25	1.03	1.07	1.34	1.19	1.05	1.31	1.14
FOCUS (MP) [31]	1.02	1.24	1.02	1.08	1.34	1.20	1.03	1.29	1.12
Diverse3D [13]	n/a	n/a	n/a	n/a	n/a	n/a	1.41	1.78	1.52
OFER-rank (ours)	**0.97**	**1.20**	**1.00**	**1.01**	**1.26**	**1.05**	**0.98**	**1.21**	**1.01**
OFER-min	0.81	1.04	0.91	0.84	1.10	0.96	0.81	1.05	0.92
OFER-avg	1.01	1.25	1.03	1.04	1.29	1.08	1.01	1.25	1.04

Table 2. **Quantitative evaluation on the NoW validation benchmark**, on the unoccluded, occluded and full subsets. "FLAME" is created by sampling random FLAME shape coefficients. Rows 2-6 show standard reconstruction methods, while the bottom rows show occlusion-based approaches. OFER-rank is our result using IdGen and IdRank networks. The bottom two rows show the minimum (OFER-min) and average (OFER-avg) reconstruction errors obtained over the 100 samples provided by IdGen. We show median (med), mean, and standard deviation (std) of the non-metrical MSE between the reconstructed and ground truth shapes.

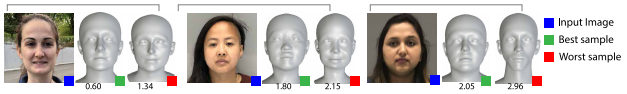


Figure 8. **Qualitative and quantitative results for best and least ranked samples** for row (b) in Tab. 1 evaluated on NoW validation images. The median MSE error between the ground truth scan and the reconstructed 3D shape is displayed below each rendering. These results demonstrate that ranking as a selection method enhances the quality of sample selection.

4.3. Evaluation on reconstructions with ExpGen

We run experiments on the full expressive reconstructions enabled by ExpGen. Similarly to IdGen, the network was trained for 400 epochs with a batch size of 128 on an RTX 8000 GPU, with the training spanning one GPU day.

Baselines and Metrics. We compare our method against the state-of-the-art diverse expression reconstruction approach by Dey et al. [13] and the single-hypothesis expres-

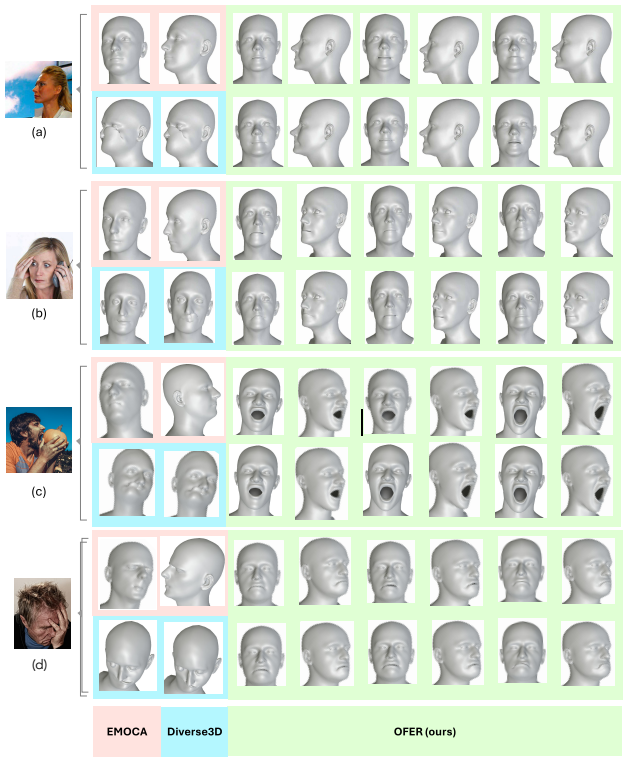


Figure 9. **Comparison of expression reconstruction for in-the-wild occluded images.** We compare against EMOCA [9] (showing front and side view, pink), two reconstructions from Diverse3D [13] (blue), and six samples (front and side view) from our method (green).

Method	N_C^{unocc}	N_C^{occ}	E_D^{occ}	E_C^{unocc}	E_C^{occ}
	RMSE ↓	RMSE ↓	RMSE ↓	RMSE ↓	RMSE ↓
Diverse3D[13]	2.44	2.16	6.4	7.46	4.72
OFER (ours)	1.90	1.95	**3.2**	**3.48**	**2.78**

Table 3. **Quantitative evaluation using SE** on unoccluded (*unocc*) and occluded images (*occ*) in Dey and CO-545 datasets. The letters represent: N for Neutral, E for expression, D for Dey dataset, and C for CO-545 dataset. Reconstructions evaluated on all front face vertices for *unocc* images and only on unoccluded vertices for *occ* images.

Method	CSE	minASD-V	maxASD-V	ASD-O	ODE	ODE-O	ODE-V
	RMSE ↓	RMSE ↓	RMSE ↓	HM ↑	max md ↓	max md ↓	max md ↓
Diverse3D[13]	0.30	1.31	1.96	0.16	0.4	0.57	0.33
OFER (ours)	**0.17**	**0.65**	**1.39**	**0.18**	**0.01**	**0.01**	**0.01**

Table 4. **Quantitative evaluation of expression reconstructions in terms of CSE, ASD-V and ODE** evaluated using CO-545 dataset. The metrics are details in Sec. 4.3

sion reconstruction method EMOCA [9]. It is important to note that Dey et al. [13] employs test-time optimization, whereas our approach does not. Additionally, their network is trained on the COMA dataset, the same dataset used in the

Method	STD-S			ODE		
	mask	*sunglasses*	*naturalocc*	*mask*	*sunglasses*	*naturalocc*
	RMSE ↑	RMSE ↑	RMSE ↑	RMSE ↓	RMSE ↓	RMSE ↓
Diverse3D[13]	11.81	21.28	20.84	0.95	0.34	0.41
OFER (ours)	**34.04**	**34.38**	**34.56**	**0.002**	**0.001**	**0.003**

Table 5. **Quantitative evaluation of expression reconstructions using STD-S and ODE metrics** evaluated on 200 images per subset (mask, sunglasses and natural occlusions) from [20].

creation of CO-545. As a result, the evaluation data overlaps with their training set, potentially giving their results an additional advantage.

Building on the metrics introduced by [54] and [13] we evaluate on six metrics: (1) Sample Error (**SE**): the average Root Mean Square Error (RMSE) between the landmark vertices of the reconstructed samples and the ground truth; (2) Closest Sample Error (**CSE**): the SE of the closest reconstructed sample; (3) Average Self Distance-Visible (**ASD-V**): to ensure that the visible regions of the reconstructions remain close to the input, the maximum distance across samples should be minimized. **maxASD-V** measures the average per-vertex RMSE on the visible regions of a sample and its "farthest" neighboring sample across all instances, while **minASD-V** measures ASD-V with the "nearest" neighbour sample; (4) Average Self Distance-Occluded (**ASD-O**): the reconstructions of *occluded* regions should show high diversity, given by $d^o = \frac{\text{RMSE}(\text{gt}^v, \text{x}_i^v)}{\max(\text{MD})^o}$, while the visible regions must remain close to the ground truth, given by $d^v = \frac{\text{RMSE}(\text{x}_i^o, \text{x}_j^o)}{\sqrt{\max(\text{MD})^o}}$. Here, $\max(MD^o)$ is the maximum mahalanobis distance threshold of the occluded vertices, and x_j is the nearest neighbour sample of x_i based on the L2 distance of occluded vertices. The superscript v and o point to the visible and occluded vertices. We compute ASD-O as the harmonic mean (HM) between d^v and d^o, given by Eq. (7); (5) Shape Standard Deviation (**STD-S**): in case of absence of ground-truth 3D data, we opt for the standard deviation metric of the entire shape, excluding data which falls outside the maximum mahalanobis distance per vertex calculated using COMA [42]; (6) Out-of-Distribution Error (**ODE**): ODE measures the average per-vertex mahalanobis distance (MD) out-of-distribution error. It addresses the observation that reconstructions from Dey et al. [13] occasionally produce non-plausible expressions that do not fall within the distribution of ground truth expressions.

$$\text{ASD-O} = \frac{2 \cdot (1 - d^v) \cdot d^o}{(1 - d^v) + d^o} \tag{7}$$

Results. The qualitative comparison of diverse expressive faces for occluded images is shown in Fig. 2 and Fig. 9. Our approach effectively generates plausible faces with varied expressions, even under challenging occlusions such as face masks. In contrast, EMOCA [9] tends to produce degenerate faces in similar hard occlusion scenarios, while Dey et

al. [13] often results in unrealistic and extreme reconstructions. The quantitative evaluation shown in Tab. 3, Tab. 4 and Tab. 5 also supports this, particularly highlighting the substantial improvement over Dey et al. [13]. We sampled 15 expressions per image for this evaluation. Our method demonstrates a significant advantage, reliably reconstructing visible regions and producing varied expressions in occluded areas.

5. Limitations and Future work

3D face reconstruction offers many valuable applications, but if not carefully regulated, it can lead to negative societal impacts, including privacy violations and misuse in surveillance, such as deepfakes or identity theft. To address these concerns, we ensured that the data we used was anonymized and that we utilized datasets that were ethically sourced.

The generative capabilities of diffusion models with diverse inputs are attributed to the amount and variations in the training data [46]. In our case, we had access to only a small subset of the available 3D supervision dataset for both IdGen and ExpGen, As a result, our generated expressions may lack certain expressive details. Therefore, a promising direction for future research is to integrate both 2D and 3D supervision to improve the performance of the method.

When we refer to performance, we specifically measure it in terms of how closely the reconstructed model approximates the ground-truth scan. Although our ranking network selects a sample that minimizes the error compared to a randomly chosen one from the generated set, it does not guarantee the selection of the absolute best match, i.e., the sample with the lowest error and closest approximation to the ground truth. From this observation we identify two potential research directions for constructing an ideal ranking network. The first is to refine the ranking architecture itself by adopting a more suitable loss function. Softmax scoring is not ideal when presented with large number of sample sets since it dilutes the scores, making it challenging to identify the best among the higher-quality samples. Additionally a more sophisticated ranking mechanism [6] can complement to the selection of quality samples. A second promising approach involves integrating the ranking process as a feedback mechanism during training of the diffusion model. Rather than using a stand-alone model, this integration could improve the quality of the generated samples, resulting in improved overall performance.

6. Conclusion

In this paper we introduced OFER, a conditional diffusion-based method for generating multiple hypotheses of expressive faces from a single-view, in-the-wild occluded image. Key to OFER is the use of two diffusion models to generate FLAME 3DMM shape and expression coefficients. To ensure a consistent geometric face shape for varied expression of a single identity, we introduced a probabilistic ranking method to select an optimal sample from the generated shape coefficients. By combining the statistical learning strengths and generative capabilities of diffusion models, along with the smooth face reconstruction provided by a parametric model, our method produces plausible 3D faces that accurately reflect the input image. OFER achieves state-of-the-art results in diverse expression reconstruction outperforming existing occlusion-based methods, and can generate plausible and diverse results for a given input.

References

[1] Oswald Aldrian. Inverse rendering of faces with a 3d morphable model. *IEEE Transactions on Pattern Analysis and Machine Intelligence*, 35:1080–1093, 2013. 2

[2] Riza Alp Guler, George Trigeorgis, Epameinondas Antonakos, Patrick Snape, Stefanos Zafeiriou, and Iasonas Kokkinos. Densereg: Fully convolutional dense shape regression in-the-wild. In *CVPR*, pages 6799–6808, 2017. 3

[3] Andrew D Bagdanov, Alberto Del Bimbo, and Iacopo Masi. The florence 2D/3D hybrid face dataset. In *Proceedings of the 2011 joint ACM workshop on Human gesture and behavior understanding*, pages 79–80, 2011. 6, 2, 3

[4] Volker Blanz and Thomas Vetter. A morphable model for the synthesis of 3D faces. In *Proceedings of the 26th Annual Conference on Computer Graphics and Interactive Techniques*, page 187–194, USA, 1999. ACM Press/Addison-Wesley Publishing Co. 2

[5] Timo Bolkart, Tianye Li, and Michael J. Black. Instant multi-view head capture through learnable registration. In *CVPR*, pages 768–779, 2023. 6, 2, 3

[6] João Brito and João Mendes-Moreira. Instance ranking with multiple linear regression: Pointwise vs. listwise approaches. In *2014 9th Iberian Conference on Information Systems and Technologies (CISTI)*, pages 1–6, 2014. 9, 2

[7] Chen Cao, Yanlin Weng, Shun Zhou, Yiying Tong, and Kun Zhou. Facewarehouse: A 3d facial expression database for visual computing. *IEEE TVCG*, 20(3):413–425, 2013. 6, 3

[8] Hang Dai, Nick Pears, William Smith, and Christian Duncan. Statistical modeling of craniofacial shape and texture. *Int. J. Comput. Vision*, 128(2):547–571, 2020. 6, 3

[9] Radek Daněček, Michael J Black, and Timo Bolkart. EMOCA: Emotion driven monocular face capture and animation. In *CVPR*, pages 20311–20322, 2022. 2, 3, 8, 5, 6

[10] Jiankang Deng, J. Guo, and Stefanos Zafeiriou. Arcface: Additive angular margin loss for deep face recognition. *2019 IEEE/CVF Conference on Computer Vision and Pattern Recognition (CVPR)*, pages 4685–4694, 2018. 3, 4, 5, 1, 2

[11] Jiankang Deng, Jia Guo, Evangelos Ververas, Irene Kotsia, and Stefanos Zafeiriou. Retinaface: Single-shot multi-level face localisation in the wild. In *Proceedings of the IEEE/CVF conference on computer vision and pattern recognition*, pages 5203–5212, 2020. 3

[12] Yu Deng, Jiaolong Yang, Sicheng Xu, Dong Chen, Yunde Jia, and Xin Tong. Accurate 3D Face Reconstruction With Weakly-Supervised Learning: From Single Image to Image Set. In *2019 IEEE/CVF Conference on Computer Vision and Pattern Recognition Workshops (CVPRW)*, pages 285–295, Long Beach, CA, USA, 2019. IEEE. 2, 3, 7

[13] Rahul Dey and Vishnu Naresh Boddeti. Generating diverse 3d reconstructions from a single occluded face image. In *CVPR*, pages 1547–1557, 2022. 2, 3, 6, 7, 8, 9, 5

[14] Haojie Diao, Xingguo Jiang, Yang Fan, Ming Li, and Hongcheng Wu. 3d face reconstruction based on a single image: A review. *IEEE Access*, PP:1–1, 2024. 2

[15] Abdallah Dib, Cedric Thebault, Junghyun Ahn, Philippe-Henri Gosselin, Christian Theobalt, and Louis Chevallier. Towards high fidelity monocular face reconstruction with rich reflectance using self-supervised learning and ray tracing. In *Proceedings of the IEEE/CVF International Conference on Computer Vision*, pages 12819–12829, 2021. 3

[16] Pengfei Dou, Shishir K. Shah, and Ioannis A. Kakadiaris. End-to-end 3D face reconstruction with deep neural networks. In *CVPR*, pages 5908–5917, 2017. 3

[17] Bernhard Egger, Andreas Schneider, Clemens Blumer, Andreas Forster, Sandro Schönborn, and Thomas Vetter. Occlusion-aware 3d morphable face models. In *BMVC*, page 4, 2016. 2, 3

[18] Bernhard Egger, Sandro Schönborn, Andreas Schneider, Adam Kortylewski, Andreas Morel-Forster, Clemens Blumer, and Thomas Vetter. Occlusion-aware 3d morphable models and an illumination prior for face image analysis. *International Journal of Computer Vision*, 126:1269–1287, 2018. 2, 3

[19] Bernhard Egger, William A. P. Smith, Ayush Tewari, Stefanie Wuhrer, Michael Zollhoefer, Thabo Beeler, Florian Bernard, Timo Bolkart, Adam Kortylewski, Sami Romdhani, Christian Theobalt, Volker Blanz, and Thomas Vetter. 3D morphable face models—past, present, and future. *ACM TOG*, 39(5), 2020. 2

[20] Mustafa Ekrem Erakın, Uğur Demir, and Hazım Kemal Ekenel. On recognizing occluded faces in the wild. In *2021 International Conference of the Biometrics Special Interest Group (BIOSIG)*, pages 1–5. IEEE, 2021. 6, 8

[21] Yao Feng, Fan Wu, Xiaohu Shao, Yanfeng Wang, and Xi Zhou. Joint 3D face reconstruction and dense alignment with position map regression network. In *ECCV*, 2018. 3

[22] Yao Feng, Haiwen Feng, Michael J. Black, and Timo Bolkart. Learning an animatable detailed 3D face model from in-the-wild images. 2021. 2, 3, 7

[23] Zhen-Hua Feng, Patrik Huber, Josef Kittler, Peter Hancock, Xiao-Jun Wu, Qijun Zhao, Paul Koppen, and Matthias Rätsch. Evaluation of dense 3D reconstruction from 2D face images in the wild. In *2018 13th IEEE International Conference on Automatic Face & Gesture Recognition (FG 2018)*, pages 780–786. IEEE, 2018. 6, 2, 3

[24] Baris Gecer, Stylianos Ploumpis, Irene Kotsia, and Stefanos Zafeiriou. Ganfit: Generative adversarial network fitting for high fidelity 3d face reconstruction. In *Proceedings of the IEEE/CVF conference on computer vision and pattern recognition*, pages 1155–1164, 2019. 2

[25] Shuguang Han, Xuanhui Wang, Mike Bendersky, and Marc Najork. Learning-to-rank with bert in tf-ranking. *arXiv preprint arXiv:2004.08476*, 2020. 3

[26] Jonathan Ho, Ajay Jain, and Pieter Abbeel. Denoising diffusion probabilistic models. *Advances in Neural Information Processing Systems*, 33:6840–6851, 2020. 2, 3, 4

[27] Harim Jung, Myeong-Seok Oh, and Seong-Whan Lee. Learning free-form deformation for 3D face reconstruction from in-the-wild images. pages 2737–2742, 2021. 3

[28] Hyeyoung Ko, Suyeon Lee, Yoonseo Park, and Anna Choi. A survey of recommendation systems: recommendation models, techniques, and application fields. *Electronics*, 11 (1):141, 2022. 3

[29] Alex Kulesza and Ben Taskar. Determinantal point processes for machine learning. *Found. Trends Mach. Learn.*, 5:123–286, 2012. 2, 3

[30] Kyungjin Lee, Juheon Yi, and Youngki Lee. Farfetchfusion: Towards fully mobile live 3d telepresence platform. In *Proceedings of the 29th Annual International Conference on Mobile Computing and Networking*, New York, NY, USA, 2023. Association for Computing Machinery. 2

[31] Chunlu Li, Andreas Morel-Forster, Thomas Vetter, Bernhard Egger, and Adam Kortylewski. Robust model-based face reconstruction through weakly-supervised outlier segmentation. In *Proceedings of the IEEE/CVF Conference on Computer Vision and Pattern Recognition*, pages 372–381, 2023. 2, 3, 6, 7

[32] Tianye Li, Timo Bolkart, Michael. J. Black, Hao Li, and Javier Romero. Learning a model of facial shape and expression from 4D scans. *ACM Transactions on Graphics, (Proc. SIGGRAPH Asia)*, 36(6):194:1–194:17, 2017. 2, 3

[33] Kevin Lin, Dianqi Li, Xiaodong He, Ming-Ting Sun, and Zhengyou Zhang. Adversarial ranking for language generation. In *Neural Information Processing Systems*, 2017. 3

[34] Tie-Yan Liu. Learning to rank for information retrieval. *Found. Trends Inf. Retr.*, 3(3):225–331, 2009. 3, 4

[35] Hai Thanh Nguyen, Thomas Almenningen, Martin Havig, Herman Schistad, Anders Kofod-Petersen, Helge Langseth, and Heri Ramampiaro. Learning to rank for personalised fashion recommender systems via implicit feedback. In *International Conference on Mining Intelligence and Knowledge Exploration*, 2014. 3

[36] Maxime Oquab, Timothée Darcet, Théo Moutakanni, Huy V. Vo, Marc Szafraniec, Vasil Khalidov, Pierre Fernandez, Daniel HAZIZA, Francisco Massa, Alaaeldin El-Nouby, Mido Assran, Nicolas Ballas, Wojciech Galuba, Russell Howes, Po-Yao Huang, Shang-Wen Li, Ishan Misra, Michael Rabbat, Vasu Sharma, Gabriel Synnaeve, Hu Xu, Herve Jegou, Julien Mairal, Patrick Labatut, Armand Joulin, and Piotr Bojanowski. DINOv2: Learning robust visual features without supervision. *Transactions on Machine Learning Research*, 2024. Featured Certification. 1

[37] Zhaoxi Pan, Song Tian, Mengzhao Guo, Jianxun Zhang, Ningbo Yu, and Yunwei Xin. Comparison of medical image 3d reconstruction rendering methods for robot-assisted surgery. In *2017 2nd International Conference on Advanced Robotics and Mechatronics (ICARM)*, pages 94–99, 2017. 2

[38] Devi Parikh and Kristen Grauman. Relative attributes. In *ICCV*, pages 503–510, 2011. 3

[39] Pascal Paysan, Reinhard Knothe, Brian Amberg, Sami Romdhani, and Thomas Vetter. A 3d face model for pose and illumination invariant face recognition. In *2009 sixth IEEE international conference on advanced video and signal based surveillance*, pages 296–301. Ieee, 2009. 3

[40] Alec Radford, Jong Wook Kim, Chris Hallacy, Aditya Ramesh, Gabriel Goh, Sandhini Agarwal, Girish Sastry, Amanda Askell, Pamela Mishkin, Jack Clark, Gretchen Krueger, and Ilya Sutskever. Learning transferable visual models from natural language supervision. In *Proceedings of the 38th International Conference on Machine Learning*, pages 8748–8763. PMLR, 2021. 1

[41] Razieh Rahimi, Ali Montazeralghaem, and James Allan. Listwise neural ranking models. In *Proceedings of the 2019 ACM SIGIR International Conference on Theory of Information Retrieval*, page 101–104. Association for Computing Machinery, 2019. 4

[42] Anurag Ranjan, Timo Bolkart, Soubhik Sanyal, and Michael J. Black. Generating 3D faces using convolutional mesh autoencoders. In *European Conference on Computer Vision (ECCV)*, pages 725–741, 2018. 2, 6, 8

[43] George Retsinas, Panagiotis P Filntisis, Radek Danecek, Victoria F Abrevaya, Anastasios Roussos, Timo Bolkart, and Petros Maragos. 3d facial expressions through analysis-by-neural-synthesis. In *Proceedings of the IEEE/CVF Conference on Computer Vision and Pattern Recognition*, pages 2490–2501, 2024. 3

[44] Olaf Ronneberger, Philipp Fischer, and Thomas Brox. U-net: Convolutional networks for biomedical image segmentation. In *Medical Image Computing and Computer-Assisted Intervention - MICCAI*, pages 234–241. Springer, 2015. 4

[45] Zeyu Ruan, Changqing Zou, Longhai Wu, Gangshan Wu, and Limin Wang. Sadrnet: Self-aligned dual face regression networks for robust 3d dense face alignment and reconstruction. *IEEE Transactions on Image Processing*, 30: 5793–5806, 2021. 3

[46] Dvir Samuel, Rami Ben-Ari, Simon Raviv, Nir Darshan, and Gal Chechik. Generating images of rare concepts using pre-trained diffusion models. In *Proceedings of the Thirty-Eighth AAAI Conference on Artificial Intelligence and Thirty-Sixth Conference on Innovative Applications of Artificial Intelligence and Fourteenth Symposium on Educational Advances in Artificial Intelligence*. AAAI Press, 2024. 9

[47] Soubhik Sanyal, Timo Bolkart, Haiwen Feng, and Michael Black. Learning to regress 3D face shape and expression from an image without 3D supervision. In *Proceedings IEEE Conf. on Computer Vision and Pattern Recognition (CVPR)*, pages 7763–7772, 2019. 2, 6, 3

[48] Matan Sela, Elad Richardson, and Ron Kimmel. Unrestricted facial geometry reconstruction using image-to-image translation. In *ICCV*, pages 1576–1585, 2017. 3

[49] Jascha Sohl-Dickstein, Eric Weiss, Niru Maheswaranathan, and Surya Ganguli. Deep unsupervised learning using nonequilibrium thermodynamics. In *International Conference on Machine Learning*, pages 2256–2265. PMLR, 2015. 4

[50] Ayush Tewari, Michael Zollhöfer, Hyeongwoo Kim, Pablo Garrido, Florian Bernard, Patrick Pérez, and Christian Theobalt. Mofa: Model-based deep convolutional face autoencoder for unsupervised monocular reconstruction. In *International Conference on Computer Vision (ICCV)*, pages 3735–3744, 2017. 3

[51] Anh Tuan Tran, Tal Hassner, Iacopo Masi, Eran Paz, Yuval Nirkin, and Gérard Medioni. Extreme 3d face reconstruction: Seeing through occlusions. In *Proceedings of the IEEE Conference on Computer Vision and Pattern Recognition*, pages 3935–3944, 2018. 2

[52] Kenny T. R. Voo, Liming Jiang, and Chen Change Loy. Delving into high-quality synthetic face occlusion segmentation datasets. *2022 IEEE/CVF Conference on Computer Vision and Pattern Recognition Workshops (CVPRW)*, pages 4710–4719, 2022. 3

[53] Erroll Wood, Tadas Baltrušaitis, Charlie Hewitt, Matthew Johnson, Jingjing Shen, Nikola Milosavljević, Daniel Wilde, Stephan Garbin, Toby Sharp, Ivan Stojiljković, et al. 3d face reconstruction with dense landmarks. In *European Conference on Computer Vision*, pages 160–177. Springer, 2022. 3

[54] Yw Yuan and Kris M. Kitani. Diverse trajectory forecasting with determinantal point processes. In *8th International Conference on Learning Representations, ICLR 2020, Addis Ababa, Ethiopia, April 26-30, 2020*. OpenReview.net, 2020. 8

[55] Xiaoxing Zeng, Xiaojiang Peng, and Yu Qiao. DF2Net: A dense-fine-finer network for detailed 3D face reconstruction. In *ICCV*, 2019. 3

[56] Tianke Zhang, Xuangeng Chu, Yunfei Liu, Lijian Lin, Zhendong Yang, Zhengzhuo Xu, Chengkun Cao, Fei Yu, Changyin Zhou, Chun Yuan, et al. Accurate 3d face reconstruction with facial component tokens. In *Proceedings of the IEEE/CVF International Conference on Computer Vision*, pages 9033–9042, 2023. 3, 7

[57] Yinglin Zheng, Hao Yang, Ting Zhang, Jianmin Bao, Dongdong Chen, Yangyu Huang, Lu Yuan, Dong Chen, Ming Zeng, and Fang Wen. General facial representation learning in a visual-linguistic manner. In *Proceedings of the IEEE/CVF Conference on Computer Vision and Pattern Recognition*, pages 18697–18709, 2022. 4, 5, 1, 2

[58] Honglei Zhuang, Zhen Qin, Rolf Jagerman, Kai Hui, Ji Ma, Jing Lu, Jianmo Ni, Xuanhui Wang, and Michael Bendersky. Rankt5: Fine-tuning t5 for text ranking with ranking losses. In *Proceedings of the 46th International ACM SIGIR Conference on Research and Development in Information Retrieval*, page 2308–2313. Association for Computing Machinery, 2023. 3

[59] Wojciech Zielonka, Timo Bolkart, and Justus Thies. Towards metrical reconstruction of human faces. In *European Conference on Computer Vision*, 2022. 2, 3, 4, 6, 7

[60] Xuan Zou, Josef Kittler, and Kieron Messer. Illumination invariant face recognition: A survey. In *2007 First IEEE International Conference on Biometrics: Theory, Applications, and Systems*, pages 1–8, 2007. 2

OFER: Occluded Face Expression Reconstruction

Supplementary Material

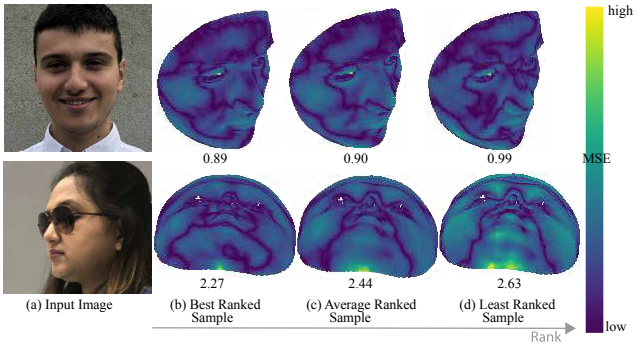


Figure 10. **Ranking on NoW validation images**. For the image in column (a), we generate 100 shape coefficients with IdGen and rank them using IdRank. Column (b) shows the top-ranked sample, (c) a mid-ranked sample (50th), and (d) the worst-ranked sample. Columns (b)-(d) show viewpoints highlighting the sample errors, with its median MSE shown underneath each sample.

#samples	Ideal lowest error sample		
	Med ↓	Mean ↓	std ↓
FLAME (Baseline)	1.02	1.30	1.11
10	0.89	1.13	0.97
50	0.83	1.07	0.94
100	0.81	1.05	0.92
500	0.78	1.02	0.90

Table 8. **Ablation on effect of sampling quantity as input to IdRank.** To evaluate the tradeoff between the number of generated samples by IdGen and the "ideal" lowest error sample in the set. The values are the lowest median error sample evaluated against the Now validation benchmark.

Embedding	Occluded subset			Unoccluded subset		
	Med ↓	Mean ↓	std ↓	Med ↓	Mean ↓	std ↓
ArcFace [10]	**1.03**	**1.26**	**1.06**	**1.01**	**1.22**	**1.01**
ArcFace+FaRL	1.05	1.30	1.09	1.03	1.28	1.06
FaRL [57]	1.15	1.40	1.12	1.07	1.30	1.06

Table 6. **Ablation on image embeddings for the IdGen network**. MSE error on the NoW validation dataset, using ArcFace [10] embedding, FaRL [57] embedding, or a combination of both.

Method	Arcface	CLIP	DINOv2
Median	1.01	1.65	1.68
Mean	1.24	2.07	2.08

Table 7. **Ablation study for IdGen embedding** on NoW validation benchmark. ArcFace trained for identity clustering performes better in comparison to other image embedding for identity recognition reconstruction task.

7. Ablation Study

We conducted several ablation studies on the choice of conditioning signal, embedding, and loss functions to optimize our model networks, which are detailed in the following sections.

7.1. Identity Generative Network (IdGen)

Choice of image embedding. The representation used for the conditioning image provided to the diffusion network plays an important role in the reconstruction task. In Tab. 6 we show ablation results for the embedding used in IdGen. The results indicate that using only the ArcFace [10] embedding improves the error metric of this network, compared to employing FaRL [57] or a combination of both as conditions. This may be because ArcFace [10] is used to distinguish identity-defining features, while FaRL [57] is designed for downstream facial analysis tasks that require capturing facial subtleties. In addition, we compare the performance of ArcFace with state of the art image embeddings, DINOv2 [36] and CLIP [40]. The results are presented in Tab. 7. The reason we hypothesize for the lower performance of CLIP and DINOv2 is that they are trained on multi-domain models and not specifically trained on faces like ArcFace.

7.2. Identity Ranking Network (IdRank)

Ranking selects low-error samples We showcase the ability of ranking network to identify subtle differences to select top-ranked sample with lower MSE error than the lower ranked samples in Fig. 10.

Sampling Quantity for Input. Naturally, increasing the number of generated samples results in a more thorough coverage of the data distribution. As the sample set size increases and leads to denser mode coverage, we expect the average error to get closer to the ground truth. However, for the ranking network to identify that optimal element, it must be be trained on a sufficiently large number of samples to effectively rank them and select the best one. This requirement comes with a significant computational costs, especially due to the slower inference time of diffusion models. Thus, finding the right balance in the number of samples used for training is important. We conducted an ablation study on different sample sizes generated by IdGen, and assessed the median error of the optimal sample from each set to determine the ideal number of samples for training IdRank. The results are presented in Tab. 8.

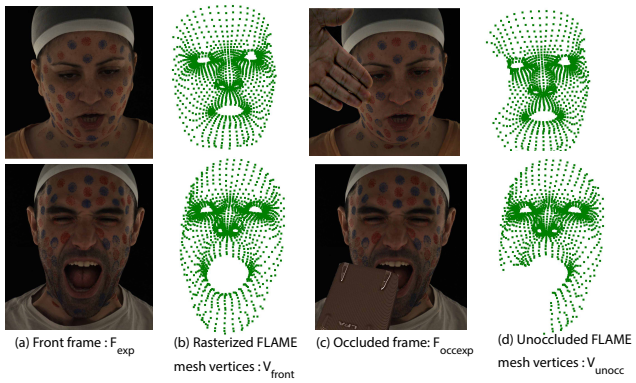


Figure 11. **CO-545.** Column (a) the expressive frames with frontal view, F_{exp}; Column (b) the rasterized the mesh vertices V_{front}; Column (c) the occluded frames with synthetic objects,F_{occexp}; Column (d) the unoccluded vertices which belong to unoccluded pixels, V_{unocc}. The pairs (F_{occexp}, V_{unocc}) make CO-545 dataset.

Input to rank network	precision ↑			IOU ↑			error (GT/Pred) (ideal = 1)		
	1 %	10 %	20 %	10 %	20 %	30 %	avg1	avg5	avg10
(a) $\hat{S}$	3.3	21.3	33.2	26.7	40.0	53.3	0.54	0.57	0.64
(b) M^{frontal}	3.3	11.3	24.8	13.3	30.0	53.3	0.49	0.58	0.61
(c) X (μ_M, M')	3.3	**44.5**	**64.7**	**33.3**	**80.0**	**93.3**	**0.68**	**0.78**	**0.83**

Table 9. **Ablation for input to ranking network.** $\hat{S}$ is the 300-dimentional shape coefficients generated from IdGen; M^{frontal} is the front face vertices of FLAME mesh M reconstructed from ($\hat{S}$; X=(μ_M, M') is the mean, residual pair defined in Sec. 3.3

Loss	precision ↑			IOU↑			error (GT/Pred)↓		
	1 %	10 %	20 %	10 %	20 %	30 %	avg1	avg5	avg10
BCE loss	0.0	3.0	20.8	0.0	0.0	16.7	0.56/0.86	0.60/0.88	0.63/0.85
Softmax loss	0.0	**30.0**	**51.7**	**50.0**	**66.7**	**66.7**	**0.58/0.76**	**0.62/0.77**	**0.65/0.79**

Table 10. **Ablation for loss function for IdRank.** We trained the network with Binary Cross Entropy (BCE) loss and Cross Entropy on Softmax (Softmax) loss using 100 Stirling(HQ) [23] frontal face images. For validation, we used 20 Florence [3] dataset frontal face images. IOU represents intersection over union of predicted ranking order and ground truth ranking order for first 10, 20 and 30 sorted rank index. error(GT/Pred) shows the average error for first 1, 5 and 10 ground truth rank samples and that of predicted rank samples.

Face vertices as Input. Selecting the most accurate sample requires a network design that excludes irrelevant information (See Sec. 3.3 for more details). To validate this claim, we conducted an ablation study comparing three inputs: (a) shape coefficients, which are a PCA model representing entire head shape; (b) all landmark vertices of the reconstructed head shape; and (c) front-face vertices from the reconstructed head shape. The results of this comparison are presented in Tab. 9. The high errors associated with the coefficients and vertex-based reconstructions likely stem from the inclusion of irrelevant information.

Loss function. The challenge in selecting the best representative shape from the samples generated by the IdGen is that, even with mild occlusions where most of the facial structure is preserved, variability can still occur. This means we need an appropriate loss function that mitigates the selection of sub-optimal samples. We considered two loss functions for this network: binary cross-entropy and softmax loss, which approximates the ground truth error distribution considering all samples. To assess the performance of both, we conducted an ablation study, the results of which are presented in Tab. 10. Since more than one sample can be optimal, ranking and selection using softmax loss yields better precision with a set of higher-ranked samples.

8. Design Choices

8.1. Ranking by distribution matching.

The objective of the ranking model is to sort the output from the network and optimize a loss based on ranking order. We choose a list-wise ranking method due to its demonstrated effectiveness [6]. Since sorting and ranking are non-differentiable operations, we reformulate the sort-rank problem into a probability distribution alignment problem aiming to minimize the softmax loss L_R between the ground truth distribution g and the predicted distribution h.

8.2. Exclusion of Ranking in Expression Generation

Our ranking network is trained to rank only *neutral* shapes and not expressions. This is because shape geometry remains consistent despite occlusions or variations in expressions in the input image. But, ranking the expression hypotheses is harder since multiple hypotheses can be equally valid for occluded regions.

9. Architecture

The detailed overview of our 1-D Unet-transformer hybrid architecture of our IdGen and ExpGen networks is shown in Fig. 12. Both share similar architecture, differing in the embeddings and the inputs. The conditional embedding of IdGen obtained from ArcFace [10] is $\mathbb{R}^{512}$, and the embedding of ExpGen obtained by concatenating ArcFace [10] and FaRL [57] embeddings is $\mathbb{R}^{1024}$.

10. Datasets

10.1. Training Dataset

In Tab. 11, we list the datasets used to train the networks in our framework. FaMoS [5] dataset comprises of 3D registered FLAME meshes. We utilized only a subset of them such that it covered all the expression variations in the entire dataset. Please note that our network trains in parametric space rather than on meshes. Therefore, we obtained the corresponding parameters for this subset directly from

Method	Median ↓ (mm)	Mean ↓ (mm)	Std ↓ (mm)
TokenFace [56]	**0.97**	**1.24**	**1.07**
MICA (8DS) [59]	1.08	1.37	1.17
3DDFA V2	1.53	2.06	1.95
DECA [22]	1.35	1.80	1.64
Dib et al. [15]	1.59	2.12	1.93
Dense landmarks [53]	1.36	1.73	1.47
FOCUS-MP [31]	1.41	1.85	1.70
Deng et al [12]	1.62	2.21	2.08
RingNet[47]	1.50	1.98	1.77
OFER (4DS) (sample selected by ranking)	1.27	1.64	1.29

Table 12. **Neutral face 3D Metrical reconstruction error on the NoW test benchmark.**. The results show comparison of accuracy of single view reconstruction methods based on NoW challenge.

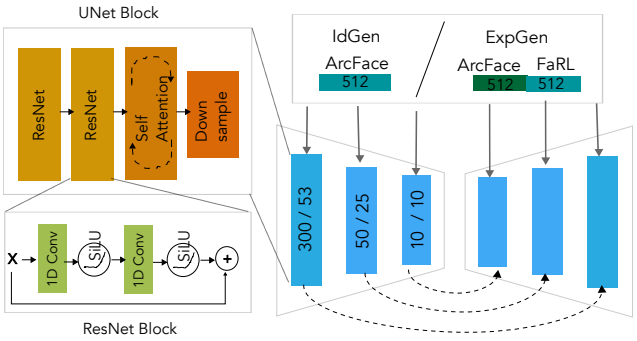


Figure 12. **1D Unet Transformer Hybrid architecture** of IdGen and ExpGen. Each block of the UNet is comprised of two resnet blocks, followed by a self-attention module and a downsampling/upsampling module for the encoder and decoder respectively. Each resnet block consists of two 1D convnet followed by SiLU activation and residual connection. For IdGen, the conditional embedding ($\mathbb{R}^{512}$) is passed to every layer of the UNet. The training input to IdGen is FLAME [32] shape coefficient, $S \in \mathbb{R}^{300}$ which gets downsampled to 50 and to 10 at the bottleneck. For ExpGen, the conditional embedding is ($\mathbb{R}^{1024}$) and the input is FLAME expression (including 3 jaw cofficients) $E \in \mathbb{R}^{53}$ which is downsampled to 25 and to 10 at the bottleneck.

Dataset	Num Subjects	Num Images	with exp
Stirling [23]	133	1322	✗
Florence [3]	53	1239	✗
Facewarehouse [7]	150	3000	✗
LYHM [8]	1211	7118	✗
FaMoS [5]	95	1.5M	✓

Table 11. **Datasets used for training Networks**. FaMoS expression coefficients are used to train ExpGen. The shape coefficients from the remaining four datasets were used to train IdGen and IdRank.

the authors of FaMoS. We used the expression coefficients from this subset to train the ExpGen. The remaining four datasets listed in the table (Stirling [23], Florence [3], Facewarehouse [7], LYHM [8]) were used to train IdGen and IdRank.

10.2. CO-545 Evaluation Dataset

We introduce a new dataset named CO-545 to quantitatively evaluate occluded expressions. First, we select the middle frame of each sequence in the COMA dataset, F_{exp}, which exhibits frontal views with expressive features while excluding neutral expressions. Subsequently, we rasterize the FLAME mesh for each frame to eliminate naturally occluded vertices from the camera's perspective, selecting only facial vertices and excluding those from the back of the head, eyeballs, neck, and ears. This subset of vertices is denoted as V_{front}. Occlusion masks [52] are then applied to the selected frames F_{occexp}, removing additional vertices from V_{front} that fall within the masked pixel areas of the image. We thus obtain the set of unoccluded vertices, denoted as V_{unocc}, for each masked image. The (F_{occexp}, V_{unocc}) pairs form the dataset, allowing us to evaluate occluded samples only within the visible regions. This procedure enables the inclusion of additional evaluation data to the dataset. A few samples from this dataset are shown in Fig. 11.

11. Additional Results.

11.1. Quantitative Results

We provide comprehensive comparison of neutral face reconstruction, including additional methods specifically focused on this task, alongside the occlusion-based reconstruction methods discussed in the main paper. Tab. 2 presents the evaluation results for non-metrical reconstruction error on the NoW [47] validation benchmark, while Tab. 12 presents metrical reconstruction error on the NoW test benchmark. We note that our method does not outperform TokenFace [56], which is explicitly trained with both 2D and 3D supervision–a limitation acknowledged and addressed as future work in the main paper. However, in the case of MICA, which when trained only on the four datasets, the results in Tab. 2 show that its performance is similar to our method. In addition, OFER demonstrates improved results when ranking is incorporated.

11.2. Qualitative Results.

We show additional expression variations from the final reconstruction of our method in Fig. 13 and Fig. 14. For identity reconstruction, Fig. 15 presents more results from the ranking of samples evaluated on the NoW validation dataset. While most of the reconstructions appear visually similar, the variations are subtle (see the forehead patterns of rows (b) and (c)). In row (c), the chin area of least ranked

sample shows high error compared to rank-1 and rank-5 samples. Since these subtle differences are hard to differentiate visually, ranking provides a way automatically select high-quality samples without manual intervention.

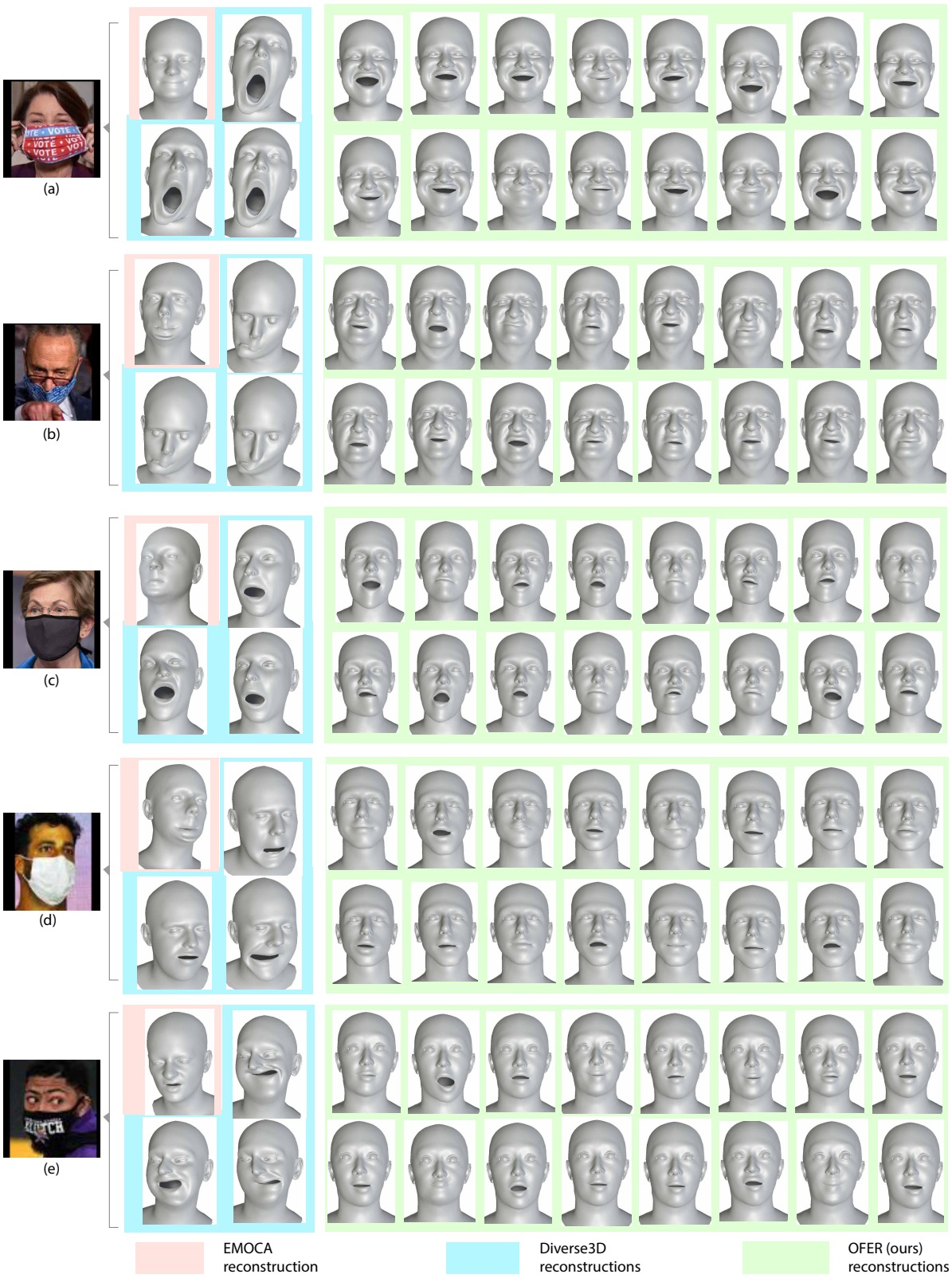


Figure 13. **Comparison of expression sampling on hard occlusions.** We compare against EMOCA [9] (pink), three samplings from Diverse3D [13] (blue) and 16 samples from our method (green).

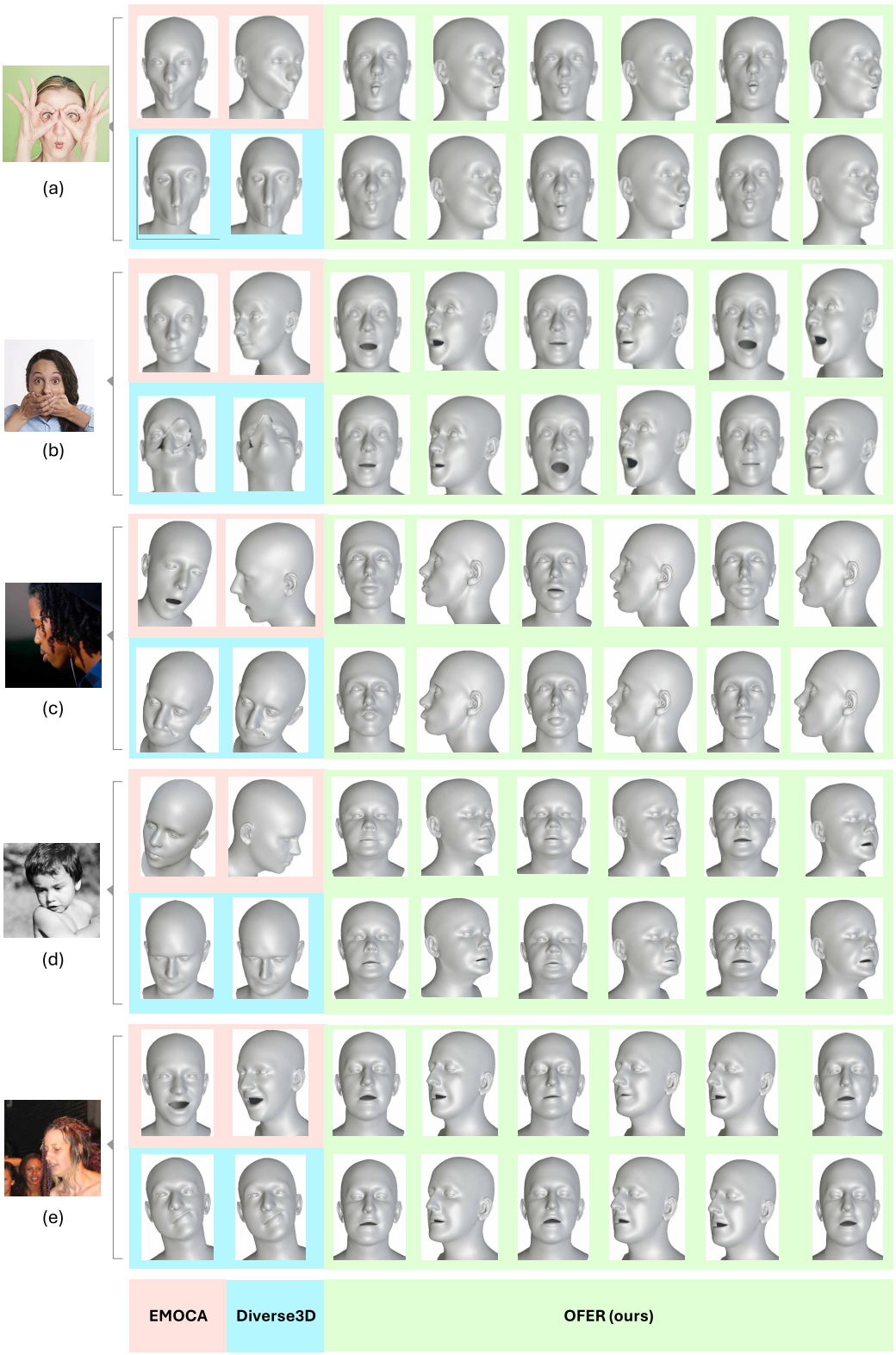


Figure 14. **Comparison of expression reconstruction for in-the-wild occluded images.** We compare against EMOCA [9] (showing front and side view, pink), two reconstructions from Diverse3D [13] (blue), and six samples (front and side view) from our method (green).

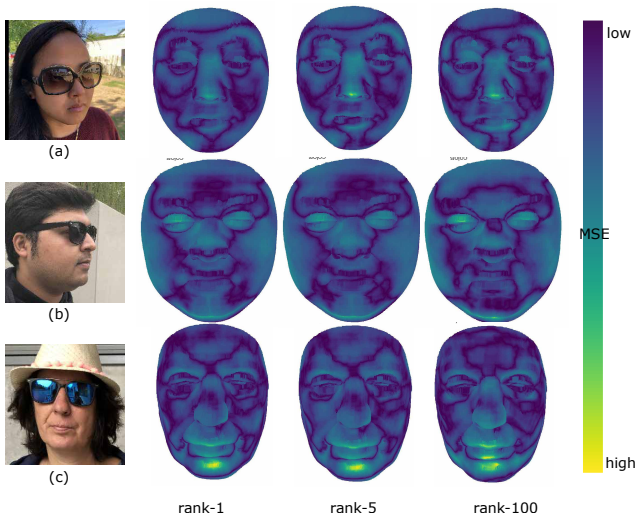


Figure 15. **Ranking on NoW validation**. Column 1 shows the optimal sample selected by IdRank, column 2 displays the sample ranked 5th, and the last column shows the lowest-ranked sample. Although error differences are subtle, variations can be observed between the higher-ranked samples (rank 1 and 5) and the lower ranked-sample (rank 100) in the nose and lip regions of image (a), the eye region of image (b), and the lip and chin region of image(c). This demonstrated the effectiveness of ranking in selecting higher-quality samples.